





Graphene decoupling through oxygen intercalation on Gr/Co and Gr/Co/Ir interfaces

Dario A. Leon ^{1,2,*} Andrea Ferretti ² Daniele Varsano ² Elisa Molinari ^{1,2} and Claudia Cardoso ^{2,†}¹*FIM Department, University of Modena and Reggio Emilia, Via Campi 213/a, Modena, Italy*²*S3 Centre, Istituto Nanoscienze, CNR, Via Campi 213/a, Modena, Italy*

(Received 17 March 2022; accepted 17 May 2022; published 6 June 2022)

We perform a density functional theory study of the effects of oxygen adsorption on the structural and electronic properties of Gr/Co(0001) and Gr/Co/Ir(111) interfaces. In both interfaces, the graphene-Co distance increases with increasing O concentration. The oxygen intercalation effectively decreases the electronic interaction, preventing the hybridization of graphene states with Co *d* orbitals, hence (partly) restoring the typical Dirac cone of pristine graphene. In the case of graphene/Co 1ML/Ir(111), which presents a moiré pattern, the interplay between the O distribution and the continuous change of the graphene-Co registry can be used to tune graphene corrugation and electronic properties. The computed electronic properties are in very good agreement with previously reported angle-resolved photoemission spectroscopy and photoemission electron microscopy measurements for Gr/Co(0001).

DOI: [10.1103/PhysRevMaterials.6.064004](https://doi.org/10.1103/PhysRevMaterials.6.064004)

I. INTRODUCTION

Graphene (Gr) grown on different transition metal (TM) substrates presents distinct structural characteristics and various alterations of its electronic properties depending on the lattice mismatch and degree of hybridization [1–16]. In particular, when grown on non-commensurate surfaces, it forms a moiré pattern and corrugates with a magnitude that depends on the interaction with the metal underneath [2,5–7]. The corrugated Gr sheet can then be used, e.g., as a template for the adsorption of molecules [6,7,17–20] as demonstrated by the deposition of TM-phthalocyanines on Gr/Co/Ir [6,7].

Considering the interfaces formed by Gr, Co, and Ir, we note that the in-plane lattice parameters of Gr and Co(0001) differ by only 0.05 Å [21–24], being in practice lattice matched. In fact, Gr grown on Co(0001) lies flat on the surface, with a small interplanar distance [9]. The electronic properties of Gr are significantly altered by the strong interaction with the Co surface [4,5,7]. On the other hand, Gr and Ir(111) lattice parameters differ by 0.25 Å [23–25] and Gr grown on Ir forms a moiré pattern corresponding to a 10×10 Gr supercell, over a 9×9 Ir supercell. The Gr-Ir distance varies slightly along the moiré structure, depending on the local Gr-Ir registry, however the electronic properties of Gr are just barely altered by the weak interaction with the substrate.

Although Co(0001) and Ir(111) have a different in-plane lattice parameter, when a single Co layer is intercalated underneath Gr grown on top of an Ir(111) layer, it assumes the lattice parameter of iridium [2,5]. In doing so, the Gr layer has an important role in stabilizing the Co single layer on the Ir surface against, e.g., the formation of Co clusters [5]. With 1 Co mono-layer (ML), the corrugation of Gr is enhanced with

respect to Gr/Ir, due to the stronger Gr-Co interaction. If a larger number of Co layers is intercalated, Co recovers its bulk structure and Gr its flat configuration [6,7].

In this scenario, oxygen intercalation constitutes an effective way to decouple Gr from a number of metal substrates [26–29]. Indeed, scanning tunneling spectroscopy data (STS) and density functional theory (DFT) results have shown that a Gr layer in the Gr/O/Ru(0001) interface is electronically decoupled from the substrate and Gr-derived π states become *p*-doped [26]. In addition, scanning tunneling microscopy (STM) experiments have shown [26] that the degree of corrugation observed upon oxygen intercalation is smaller than for the pristine Gr/Ru(0001). Likewise oxygen intercalation decouples effectively Gr from Ni(111) [27], quenching the strong substrate-adsorbate interaction with the formation of a thin Ni oxide layer at the interface. Angle-resolved photoemission spectroscopy (ARPES) measurements on pristine Gr/Ni(111) show that the Gr π band is shifted towards higher binding energy by about 2.5 eV with respect to the position of free-standing Gr, and the Dirac cone dissolves into the metal 3*d* bands. Upon oxygen intercalation the hybridization with Ni 3*d* states is removed and the characteristic shape of the Dirac cone is restored and identifiable near the Fermi level [27].

Regarding Gr/Co, one of the systems under consideration in this work, recent studies based on x-ray photoemission spectroscopy (XPS), photoemission electron microscopy (PEEM), and ARPES measurements on graphene epitaxially grown on Co(0001) [28,29] show that, upon O intercalation, there is an effective electronic decoupling between Gr and Co. In fact, for an O coverage of 0.5 ML the Gr C_{1s} peak shifts by 1.1 eV to lower binding energies and valence band mapping reveals that the Gr band structure acquires a nearly free-standing character with a small *p* doping. Interestingly, it has also been shown that the O adsorption can be reversed upon annealing [29].

*darioalejandro.leonvalido@cnr.nano.it

†claudia.cardoso@nano.cnr.it

When Co is exposed to oxygen both physical adsorption and oxidative processes may occur [30,31]. While low exposures result in chemisorbed oxygen coupled ferromagnetically with the substrate [32,33], when the oxygen exposure increases, cobalt oxide may form in two different stoichiometries: CoO or, in smaller proportion, Co₃O₄. A theoretical study [31], investigating the surface and subsurface oxygen adsorption on Co(0001) over a wide coverage range from 0.11 to 2.0 ML, shows that the coverage with the highest adsorption energies is 0.25 ML, whereby the O atoms are adsorbed on the surface. For larger exposures, O begins to penetrate into the surface. In the same study, the energetics of O adsorption and the structural and electronic properties of the surface are discussed in detail. Similarly, Gr@Co interfaces can adsorb oxygen under Gr in a stable way [28–30,34]. However, the mechanisms and structural details of O adsorption on Co depend sensitively upon the experimental parameters [30,34], on the epitaxial relation between graphene and the substrate, and on the concentration of holes (carbide islands) in the graphene layer [29]. In the case of epitaxially oriented graphene, the holes in the layer act as intercalation centers.

The aim of the present work is to investigate, by means of first principles calculations, how the Gr-Co hybridization, and therefore, graphene electronic properties, change due to oxygen intercalation and, in the case of a moiré structure, how the graphene corrugation pattern is influenced by the intercalation of oxygen. We start by discussing the O adsorption on Co(0001) and Co/Ir(111) surfaces and then we consider the effects of O intercalation under graphene in both Gr/Co(0001) and Gr/1 ML Co/Ir(111) interfaces, focusing on the Gr-Co hybridization. We compute the band structure of Gr/Co(0001) before and after O adsorption and compare the results with recent ARPES and PEEM measurements [28,29]. For the case of Gr/1 ML Co/Ir(111), we analyze how Gr corrugation is affected by the O intercalation and its dependence on the O distribution and concentration.

The paper is organized as follows. In Sec. II, we describe the adopted computational methodology. In Sec. III A, we present the results regarding the energetics of the different O adsorption sites on Co and Co/Ir surfaces. In Sec. III B, the electronic properties of the most stable systems are investigated, and finally the effect of O intercalation on the Gr/Co interaction is discussed in Sec. III C for the Gr/Co and in Sec. III D for the Gr/1ML Co/Ir interfaces.

II. METHODS

We have performed DFT calculations on Co(0001) and Co/Ir(111) slabs, with and without adsorbed oxygen, as well as on the Gr/O/Co(0001) and Gr/O/1 ML Co/Ir(111) interfaces. Co and Ir bulk systems were also computed with consistent parameters for completeness. All calculations were performed using the plane wave and pseudopotential implementation of DFT provided by the QUANTUM ESPRESSO package [35,36]. We employed the GGA-PBE [37] exchange-correlation functional and adopted ultrasoft (US) pseudopotentials to describe electron-ion interactions. The kinetic energy cutoff was set to 30 Ry for the wave functions and 330 Ry for the charge density. For the Gr/O/Co(0001) and

Gr/1 ML Co/Ir(111) interfaces, van der Waals interactions were taken into account through the Grimme-D3 scheme [38].

The metallic substrates were modeled by considering slabs of 5 atomic layers, referred in the text as Co(0001)₅ and Co₁/Ir(111)₄, with a vacuum layer of at least 10 Å in order to prevent spurious interactions between the replicas. An additional 2 Å of vacuum was introduced in the modeling of the surfaces in the presence of oxygen. The slab thickness of 5 layers was validated by calculating adsorption energies considering up to 9 layers as reported in Ref. [39]. The Brillouin zone was sampled by using **k**-point meshes of 16 × 16 × 16 for cobalt and iridium bulk, 16 × 16 × 1 for Co(0001) and Co/Ir(111) surfaces, and 8 × 8 × 1 for surfaces with adsorbed oxygen. The projected density of states for Gr/O/Co(0001) was computed with a 40 × 40 × 1 **k** grid.

We have considered oxygen concentrations of 0.25 and 0.5 ML, that, according to Ref. [31], are below the values required to form cobalt oxide and for which the oxygen atoms remain chemisorbed on the surfaces. In order to model these oxygen coverages, we have used $p(2 \times 2) - \text{O}$ and $p(2 \times 2) - 2\text{O}$ slab supercells. The initial positions for the oxygen atoms were chosen according to the most stable configurations reported in Ref. [31] and are shown in Fig. 1, where we have also labeled the O sites following the notation of Ref. [31]. All the atomic positions (O, Co, and Ir) were then optimized until the forces acting on atoms were smaller than 1.0×10^{-4} Ry/Bohr.

The Gr/1 ML Co/Ir(111) interface was simulated considering the complete moiré-induced periodicity by using a 9×9 supercell of Ir(111), corresponding to a 10×10 supercell of pristine Gr, adding up to a supercell with more than 600 atoms. The lattice parameters were obtained by relaxing Ir bulk at the same level of theory, corresponding in 9×9 periodicity to a hexagonal cell of 46.54 Bohr radius for the moiré structure. The metal slab of the Gr/1 ML Co/Ir(111) interface was modeled with four metallic layers (3 Ir plus one Co layer) with an added layer of H atoms on the bottom surface. The H layer was added in order to cancel possible interactions between states on the two surfaces due to the finite thickness of the slab, and stabilize convergence by avoiding metastable magnetic states (more details are given in Ref. [39]). Atomic positions were then fully relaxed, except for the two bottom Ir layers and the H saturation layer, until ionic forces were smaller than 0.001 Ry/Bohr. The Brillouin zone was sampled with a 2×2 grid of **k** points.

The oxygen adsorption energies on Co(0001) and Co/Ir(111) surfaces, E_{Co}^{O} and $E_{\text{Co/Ir}}^{\text{O}}$, are defined as the difference between the total energy of the target system with the adatoms and the energy of the clean surface plus half the energy of an oxygen molecule:

$$E_{\text{Co}}^{\text{O}} = -\frac{1}{N_{\text{O}}} \left(E_{\text{O/Co}} - E_{\text{Co}} - N_{\text{O}} \frac{1}{2} E_{\text{O}_2} \right), \quad (1)$$

$$E_{\text{Co/Ir}}^{\text{O}} = -\frac{1}{N_{\text{O}}} \left(E_{\text{O/Co/Ir}} - E_{\text{Co/Ir}} - N_{\text{O}} \frac{1}{2} E_{\text{O}_2} \right), \quad (2)$$

where N_{O} is the number of oxygen atoms in the supercell, and $E_{\text{O/Co}}$, E_{Co} , and E_{O_2} are the total energy of the adsorbate+substrate system, pristine surface, and a free oxygen molecule, respectively. In principle, O adsorption energies

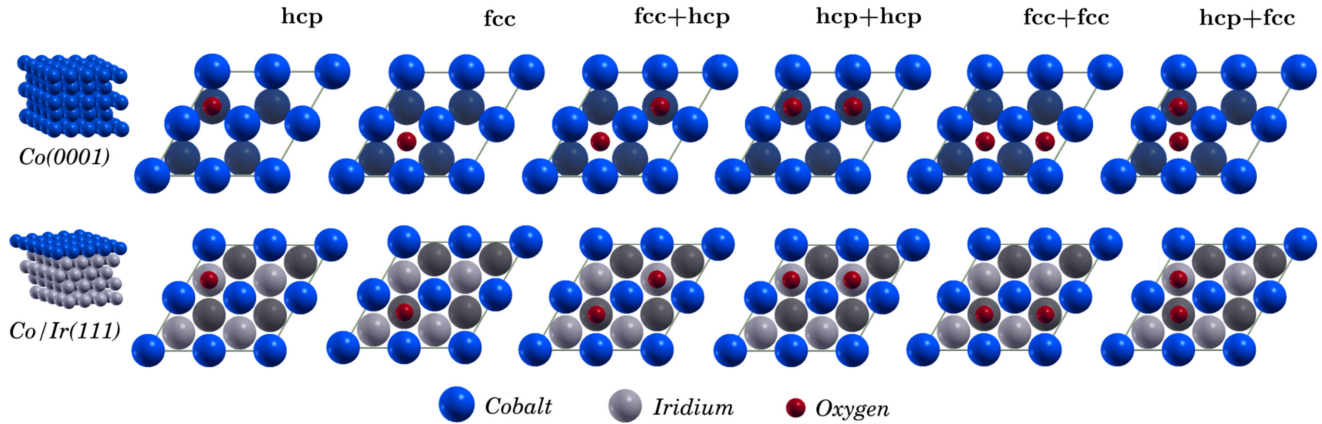


FIG. 1. Top view of the different O adsorption sites considered in the calculations, for the Co (top) and Co/Ir surfaces (bottom), for 0.25 and 0.5 ML O concentrations. The labeling of the different configurations follows the notation used in Ref. [31]. The notation refers to surface adsorption sites.

could also be referred to the energy of the free oxygen atom, resulting in an overall increase of the adsorption energies, without altering the trends [31], of 2.87 eV.

III. RESULTS AND DISCUSSION

A. Oxygen adsorption energies on Co and Co/Ir surfaces

We start by discussing the adsorption of oxygen on Co and Co/Ir interfaces. The two systems most striking difference is that 1 ML Co is epitaxial on Ir(111), resulting in a stretched lattice parameter with respect to thick Co(0001) films. We compute the adsorption energies for oxygen adsorbed on a 5-layer Co slab ($\text{Co}(0001)_5$) and on a slab with a layer of Co on top of a 4 Ir layers ($\text{Co}_1/\text{Ir}(111)_4$), for both 0.25 and 0.5 ML coverage, corresponding to one or two O atoms in a 2×2 cell, respectively. We consider different possible adsorption sites as illustrated in Fig. 1, whose calculated adsorption energies are reported in Table I.

For the lowest oxygen coverage on $\text{Co}(0001)_5$, 0.25 ML, the two adsorption sites, fcc and hcp present very similar adsorption energies, 2.56 and 2.60 eV, respectively. The adsorption energy drops to values around 2.13 eV for the 0.5 ML coverage, indicating a repulsive interaction between O adatoms. The most favorable adsorption configuration is the one labeled hcp+hcp, differing by less than 0.01 eV from the fcc+hcp configuration (see Fig. 1), although such a small energy difference is at the verge of the accuracy of our com-

putational approach, such that both sites can be considered energetically equivalent (more details in Ref. [39]). Overall, the present results compare well with the values previously reported in Ref. [31], with both the adsorption energy and the energy differences between different configurations decreasing when increasing O concentration.

In the case of $\text{Co}_1/\text{Ir}(111)_4$, for 0.25 ML, the configuration with the lowest energy corresponds to the O atom adsorbed on a fcc site. The adsorption energy is 2.89 eV, 0.04 eV larger than for the hcp configuration. As in the case of the Co surface, the adsorption energy decreases with increasing O content. The most favorable configuration is then the fcc+fcc, followed by the fcc+hcp configuration, with an adsorption energy of 2.64 and 2.55 eV, respectively. In general, the most favorable site for oxygen adsorption on $\text{Co}(0001)$ slabs is hcp, whereas oxygen tends to adsorb on the fcc site for Co/Ir. Comparing the two surfaces, we find that the adsorption energies of oxygen for both 0.25 and 0.5 ML are respectively 0.29 and 0.45 eV larger on Co/Ir than on Co.

The computed distances between the oxygen adatoms and the surface are reported in Table II as d_O . For the 0.25 ML configurations, the higher the adsorption energy the closer the oxygen atoms are to the surface. The two configurations of adsorbed O on $\text{Co}(0001)$ show similar O-surface distances, that differ in less than 0.06 Å, while on Co/Ir the differences are larger, 0.14 Å. For 0.5 ML, the O-surface distances, for both $\text{Co}(0001)_5$ and $\text{Co}_1/\text{Ir}(111)_4$, have a larger dependence on the adsorption site, with no apparent correlation between the O-surface distances and the adsorption energies, probably due to the O-O interaction. Comparing the lowest energy configurations of each surface, the oxygen atoms are closer to the surface on Co/Ir than on Co, consistently with its larger in-plane lattice parameter.

Oxygen adsorption affects also the layer-layer distance in the metallic slabs, as shown in Table II, with an increase of the first interlayer distance d_{z1} on both $\text{Co}(0001)_5$ and $\text{Co}_1/\text{Ir}(111)_4$, with the O concentration. In contrast, the distance between the second and third layers d_{z2} presents a slightly decrease.

We have also studied configurations with the oxygen atoms inside the metal surface. For both $\text{Co}(0001)_5$ and

TABLE I. Adsorption energies, in eV/O, computed for $\text{Co}(0001)_5$ and $\text{Co}_1/\text{Ir}(111)_4$. For the sake of comparison, we show in brackets the results from Ref. [31].

O coverage	O site	$\text{Co}(0001)_5$	$\text{Co}_1/\text{Ir}(111)_4$
0.25 ML	hcp	2.60 [2.67]	2.85
	fcc	2.56 [2.66]	2.89
0.5 ML	fcc+hcp	2.18 [2.13]	2.55
	hcp+hcp	2.19 [2.09]	2.53
	fcc+fcc	2.13 [1.97]	2.64
	hcp+fcc	1.78 [-]	2.22

TABLE II. Oxygen-substrate (d_0) and interlayer distances (d_{z1} , d_{z2}) for Co(0001)₅ and Co₁/Ir(111)₄. For the Co(0001)₅ surface, the interlayer distances correspond to the distances between Co neighboring layers. For the Co₁/Ir(111)₄ surfaces, the first interlayer distance d_{z1} corresponds to the distance between the Co layer and the next Ir layer, while the second one (d_{z2}) corresponds to an Ir-Ir layer distance. All the reported distances are in Å and were computed considering the difference between the average vertical coordinate of each atomic layer.

O coverage	O site	Co(0001) ₅			Co ₁ /Ir(111) ₄		
		d_0	d_{z1}	d_{z2}	d_0	d_{z1}	d_{z2}
pristine	–	–	3.69	3.83	–	3.82	4.33
0.25 ML	hcp	2.12	3.75	3.80	1.98	3.89	4.31
	fcc	2.18	3.78	3.78	1.84	3.90	4.30
0.5 ML	fcc+hcp	2.24	3.86	3.76	1.92	3.95	4.29
	hcp+hcp	2.07	3.82	3.78	1.90	3.94	4.30
	fcc+fcc	2.06	3.87	3.75	1.80	3.97	4.29
	hcp+fcc	2.22	3.90	3.78	1.88	3.97	4.29

Co₁/Ir(111)₄, and for both O concentrations considered, the added O always migrates to the surface. The one exception is a configuration with O occupying an fcc site below the second metal layer. However, this subsurface configuration has an adsorption energy that is considerably smaller than the surface configurations. In fact, subsurface O adsorption is expected to occur only for O contents larger than 1 ML [31]. In Ref. [31], oxygen is found below the first layer, but this contrast may be justified, e.g., by differences in the relaxation process. We report more details about the subsurface configurations in Ref. [39].

B. Electronic and magnetic properties

In order to understand the influence of O on the Co electronic properties, in Fig. 2, we report the density of states projected on the O and the top layer Co atoms (pDOS). Majority and minority spin bands are shown for 0.25 and 0.5 ML coverage, for both Co(0001)₅ and Co₁/Ir(111)₄, and compared with the pristine systems (displayed in grey). The DOS computed for the clean systems show the Co 3d states localized around the Fermi energy (E_F), with a spin split of about 2 eV, that results in a magnetic moment of 1.68 μ_B /Co for Co(0001)₅ and 2.02 μ_B /Co for Co₁/Ir(111)₄. The majority spin d-states are completely occupied, whereas the minority DOS cuts through the Fermi level, with peaks above and below, and a valley at Fermi for both systems.

The Co₁/Ir(111)₄ shows a narrower DOS than Co(0001)₅, leading to larger magnetic moments. This enhancement is related to some degree of confinement induced when going from a Co slab to a single layer on Ir [7] as well as to the stretched lattice parameter of Co 1ML due to the presence of Ir(111). The same narrowing of the DOS leading to large magnetic moments was reported also for the Gr/Fe/Ir [14] and Gr/FeCo/Ir [40] interfaces, both from experiment and DFT calculations. It is worth noticing, though, that these calculations were performed within DFT+ U [41] and that the choice for the Hubbard U parameter affects the computed magnetic

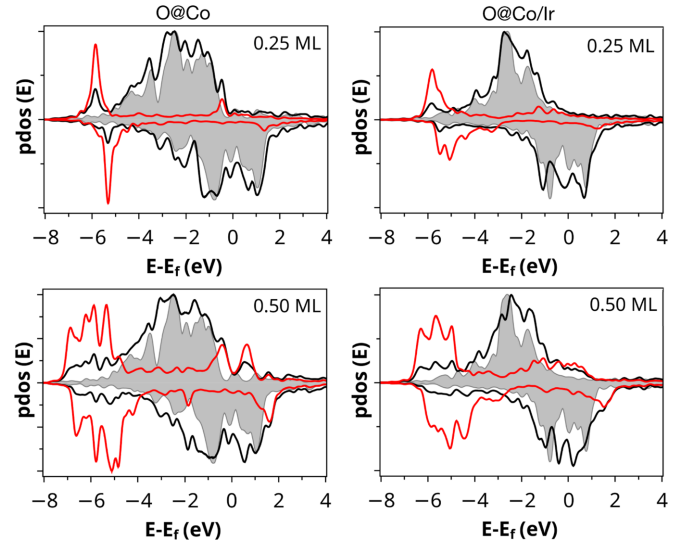


FIG. 2. Density of states computed for O@Co (left) and O@Co/Ir (right), for 0.25 (top), and 0.5 ML (bottom). The density of states is projected on the atomic orbitals of O (red lines) and Co on the top layer (black lines). The Co top layer DOS for the pristine surface is shown in grey.

moments, as described in detail in the Supplementary material of Ref. [40].

In the presence of O adatoms, there is a clear overlap between Co and O states that induces a spin-split of the latter. The O 2p states hybridize with the lowest edge of the Co 3d bands, resulting in a peak around 5.5 eV below the Fermi level. There is a second state, with the majority spin located just below the E_F and the minority spin about 1.5 eV above in the case of the 0.25 ML, more pronounced for Co(0001)₅ rather than Co₁/Ir(111)₄. For the 0.5 ML, the O pDOS becomes wider and shifts slightly downward (i.e. towards larger binding energies) reaching to 6.8 eV, due to the O-O repulsive interaction, in agreement with Ref. [31]. Comparing the Co(0001)₅ and Co₁/Ir(111)₄ surfaces, there are evidences of a larger hybridization of the O atom with Co states in the case of Co₁/Ir(111)₄, for which the O pDOS peaks are broader, consistently with the larger O adsorption energies mentioned above.

In Table III, we show a summary of the magnetization and magnetic moments obtained for O adsorbed on the Co(0001)₅ and Co₁/Ir(111)₄ slabs. In all configurations, the O moment is aligned ferromagnetically with Co. For the pristine systems, the average magnetic moment of the top layer Co atoms is larger for Co₁/Ir(111)₄ than for the Co(0001)₅ slab, 1.92 and 1.76 μ_B respectively, reflecting the narrower structure of the DOS observed for Co₁/Ir(111)₄. After oxygen adsorption, a small magnetic moment is found on the O atom, with values ranging from 0.08 to 0.27 μ_B on Co(0001)₅, and from 0.26 to 0.43 μ_B , on Co₁/Ir(111)₄, depending on the oxygen concentration. However, chemisorbed oxygen atoms have a very small impact on the total magnetization of the Co and Co/Ir slabs since the moments of the Co atoms in the first layer, (m_{Co} in Table III), tend to decrease with respect to the pristine systems. The effect is slightly larger for Co₁/Ir(111)₄ since it has only one magnetic layer (i.e., the top Co layer). Among

TABLE III. Total magnetization (in units of Bohr magneton) per cobalt atom (m_{tot} , in μ_B/Co), average magnetic moment for the Co atoms in the first layer (m_{Co}), and average O magnetic moment (m_{O}), computed for O adsorbed on $\text{Co}(0001)_5$ and $\text{Co}_1/\text{Ir}(111)_4$, for both the 0.25 and 0.5 ML coverage.

O coverage	O site	$\text{Co}(0001)_5$			$\text{Co}_1/\text{Ir}(111)_4$		
		m_{tot}	m_{Co}	m_{O}	m_{tot}	m_{Co}	m_{O}
pristine		1.68	1.76	–	2.02	1.92	–
0.25 ML	hcp	1.68	1.69	0.23	2.07	1.89	0.37
	fcc	1.70	1.72	0.26	2.06	1.85	0.31
0.5 ML	fcc+hcp	1.61	1.24	0.08	2.02	1.73	0.37
	hcp+hcp	1.67	1.49	0.18	2.12	1.80	0.33
	fcc+fcc	1.68	1.53	0.19	1.94	1.68	0.26
	hcp+fcc	1.71	1.64	0.27	2.29	1.93	0.43

the most energetically stable configurations, the magnetic moment varies less than 5%.

Cobalt oxide bulk (CoO) is known to have an antiferromagnetic (AF) order, that has been well-described at the DFT+ U level, e.g., in Refs. [42–46]. This motivated the search for possible antiferromagnetic configurations also for the surfaces studied in this work. In this case, the only AF solutions were found for two Co/Ir configurations, with O adsorbed on hcp+hcp and fcc+fcc. However these configurations have a total energy that is 0.3 eV/O higher than the ferromagnetic configuration, being thereby significantly less stable. More details are provided in Ref. [39].

C. Graphene on Co: Decoupling through O intercalation

Having established structural, electronic, and magnetic properties of oxygen adsorbed on Co and Co/Ir, now we consider the case of graphene (Gr) adsorbed on $\text{Co}(0001)$ and $\text{Co}/\text{Ir}(111)$, in the presence of O intercalation. In particular, we take advantage of the structural analysis performed in Sec. III A to build the models for $\text{Gr}/\text{O}/\text{Co}(0001)$ and $\text{Gr}/\text{O}/\text{Co}/\text{Ir}(111)$. XPS, PEEM, and ARPES measurements on $\text{Gr}/\text{Co}(0001)$ show that, upon O intercalation, there is an electronic decoupling between graphene and Co, and that the graphene band structure acquires a nearly free-standing character except for a small p -doping [28,29]. In order to assess the effect of oxygen intercalation under Gr, we have performed calculations for graphene on $\text{Co}(0001)_5$, with and without O adsorbed under graphene. We consider an oxygen coverage ranging from 0.0625 to 0.5 ML.

In Fig. 3, we show, in red, the adsorption energy, which increases for increasing O concentration. For 0.25 and 0.5 ML, the adsorption energies are 2.11 and 2.21 eV, respectively, similar to the values computed without the graphene layer (2.60 and 2.19 eV). However, without graphene the adsorption energy for 0.25 ML is slightly larger than the one for 0.5 ML, which indicates that the graphene layer partially screens the interaction between neighboring oxygen atoms.

Concerning structural properties, in Fig. 3, we show the change of the average distance between graphene and the Co surface. We observe that oxygen adsorption has a large impact on the structure of the Gr/Co interface yielding a dramatic

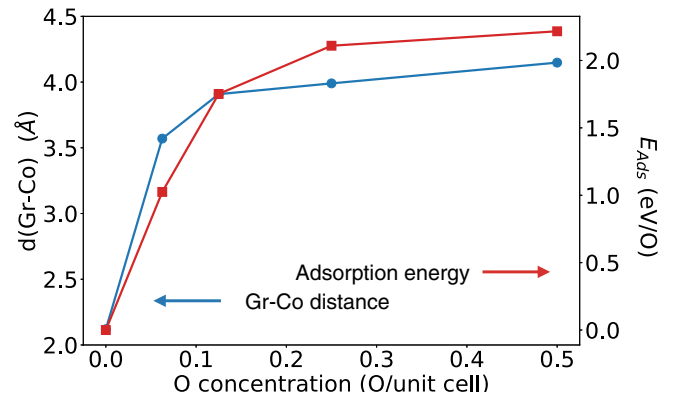


FIG. 3. Gr-Co distance (blue line, left scale) and corresponding adsorption energy (red line, right scale), computed for different O concentrations.

increase in the graphene-Co distance, that changes from 2.1 Å in the pristine case to 4.1 Å upon the adsorption of 0.5 ML of O. Moreover, even the smallest O concentrations considered here lead to a significant increase on the Gr-Co distance. In Fig. 4, we also present the density of states computed for the pristine GrCo interface and upon O adsorption, again with a 0.25 ML concentration. In the absence of oxygen, a clear hybridization between Co d electrons and C states close to the Fermi level can be seen from the projected density of states of Gr@Co , as shown in the left panel of Fig. 4, and as already observed in Refs. [4,5,47]. In the presence of adsorbed oxygen, the pDOS of C atomic orbitals is similar to that of freestanding graphene.

In Fig. 5 (left panel), the bands computed for the 2×2 Gr@Co unit cell are mapped into the $\text{Gr} 1 \times 1$ Brillouin zone by using the UNFOLD-X code [48]. This procedure allows us to visualize an effective band structure corresponding to the graphene unit cell in the presence of substrates and adatoms. Similarly to what found in Refs. [14,40] for the GrCoIr interface in a 10×10 Gr supercell, the Dirac cone is disrupted by the hybridization of Gr with the Co d states, and the C states show a spin-split induced by the spin-polarized Co states. Overall, this results into a shift of the apex of the cone of about -3.7 and -2.9 eV for the majority and minority spin channels, respectively (left panel of Fig. 5).

At variance with Gr@Co , for $\text{Gr@O}/\text{Co}$ (right panel of Fig. 5) the Dirac point can be recognized slightly above the Fermi level, at about 0.4 eV, indicating a small doping of graphene, in excellent agreement with the value of 0.3 eV recently measured by ARPES experiments [28], and the 0.4 eV value from the PEEM momentum map reported in Ref. [29]. The same type of doping is also seen in Gr@Ir [47,49] and in $\text{Gr}/\text{Ru}(0001)$ upon O intercalation [26], with the Dirac cones located at $+0.21$ and $+0.5$ eV, respectively.

The oxygen adsorption also changes the magnetic moments of the interface. Without O, the average magnetic moment of Co is $1.7 \mu_B$, but the hybridization with graphene decreases the moment of the Co top layer. In fact, the average magnetic moment increases from 1.6 to $1.8 \mu_B$ when going from the top to the fourth Co layer, in good agreement with the values estimated from x-ray magnetic circular dichroism,

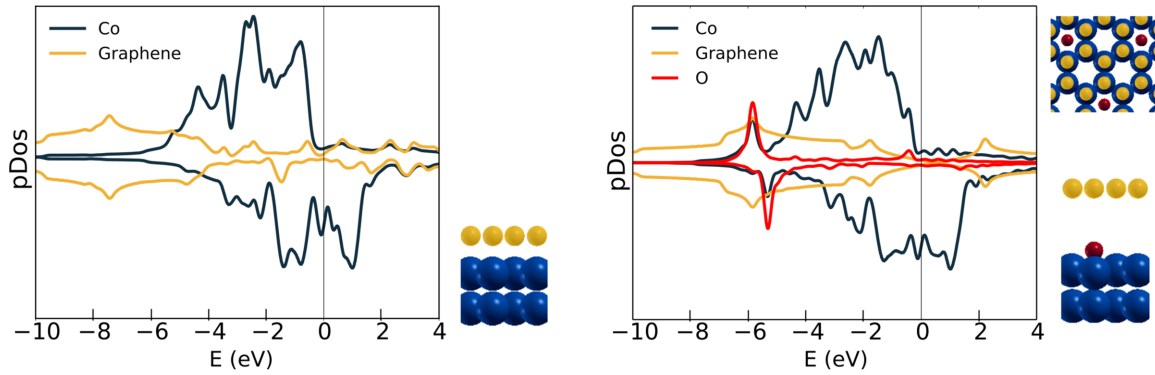


FIG. 4. Density of states computed for Gr@Co (left) and Gr@O/Co (right) and projected on the C, on the first layer Co and O atomic orbitals. Next to each plot, a scheme with the atomic structure, illustrating the difference in the Gr-Co distance for the two systems and, for the case of Gr@O/Co, a top view showing the O distribution.

$\mu_s = 1.47\mu_B$ [29]. Concerning graphene, there is a small magnetic moment induced in the two nonequivalent C atoms, -0.08 and $0.05\mu_B$. Upon O adsorption the Co magnetic moment is more uniform across the layers, with an average of $1.7\mu_B$, and there is no significant moment on graphene. The adsorbed O atom has a magnetic moment of $0.2\mu_B$, in the same range of the ones computed without the graphene layer.

D. Graphene on CoIr Interplay between O and the Gr-Co registry

We will now focus on the effects of O intercalation on the Gr/1 ML Co/Ir(111) interface. As mentioned before this interface presents a moiré structure corresponding to a 10×10 Gr supercell on top of a 9×9 Ir supercell, intercalated by 1 ML Co with a structure similar to Ir, as illustrated in Fig. 6. The graphene sheet presents a corrugation caused by the fact that the Gr-Co distance depends on the registry between the two layers [5], which varies continuously through the moiré unit cell. According to the present results, when Gr sits on

top of a Co atom, the Gr-Co distance is minimum, with a value of 1.94 \AA and the largest Gr-Co distance is of 3.5 \AA and corresponds to hollow sites (fcc/hcp stacking). This results in a corrugation of the Gr sheet of 1.59 \AA , in good agreement with the literature [2,6,7,50].

We performed a similar geometry optimization of the interface before and after O adsorption. We have considered a uniform distribution of O in the supercell corresponding to a concentration of 11%. The computed adsorption energy is 1.17 eV/O , slightly smaller than the Gr/Co(0001) value interpolated for the same O concentration, 1.6 eV/O . The optimized structures are illustrated in Fig. 6. The comparison of the two interfaces shows, as for the case of the Gr/Co(0001) interface, that O causes an increase of the average Gr-Co distance from 2.24 \AA in the pristine case to 2.96 \AA upon O intercalation, and a change on the structure of Gr corrugation. Despite this increase, the small O concentration and the particular atomic distribution considered in the present calculations allows for some regions, corresponding to C sites on top of Co atoms, to preserve a small Gr-Co distance, which also results in a slight increase in the corrugation, from 1.59 \AA in the pristine case to 1.74 \AA .

This would depend on the O distribution on the surface and we expect that, for large enough O concentrations the Gr layer completely decouples from the Co surface, regaining its free standing properties, as seen in the previous section for the Gr/Co(0001) interface. In Fig. 7, we show the projected density of states corresponding to these geometries. Comparing with the DOS obtained with and without O intercalation, shown in the left panel of Fig. 4, a small O concentration already results in a partial recover of the Gr free standing character, with a decrease of its spin polarization, even if there are still signs of Gr-Co hybridization.

IV. CONCLUSIONS

In this work, we study, by means of DFT calculations, the effects of oxygen intercalation on the electronic properties of the Gr/Co(0001) and Gr/Co/Ir(111) interfaces. In the first part of the work, we disregard the presence of graphene and we study two different surfaces in the presence of oxygen adatoms: Co(0001) and a single layer of Co deposited on of Ir(111), taking into account that in the latter case the single Co

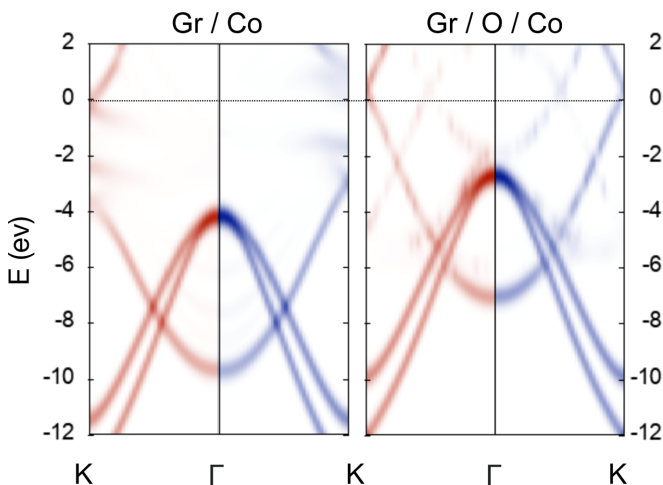


FIG. 5. Bands projected on the atomic orbital of graphene, computed for Gr@Co (left) and Gr@OCo (right) unfolded in the graphene unit cell. The red and blue colors correspond to the spin up and spin down states.

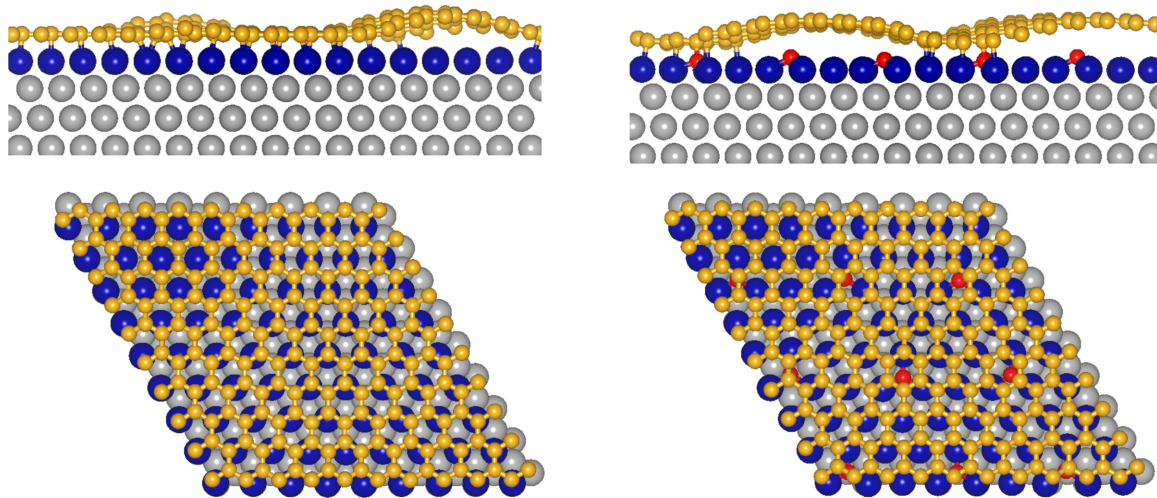


FIG. 6. Scheme of the crystal structure as computed within DFT for Gr/1ML Co/Ir before and upon O adsorption, with a O concentration of 11%.

layer is epitaxial on Ir(111) [2,5], and therefore has a lattice parameter 0.25 Å larger than that of the Co(0001) surface. In particular, this allows us to address the effect of the strain on the absorption of oxygen on Co. The adsorption energies are about 0.3 eV larger for Co/Ir(111) than for the Co(0001) surface and, in both structures, the adsorption energies decrease with increasing O content.

Regarding the electronic properties, upon adsorption there is a clear hybridization between O and Co states, that is larger in the case of Co/Ir(111). The larger magnetic moment of the Co single layer when deposited on Ir, a consequence of its strained lattice, also results in a slightly larger O magnetic moment.

Finally, we have addressed the effect of O intercalation in the Gr/Co(0001) and Gr/Co/Ir(111) interfaces. The present results show that O adsorption induces an increased graphene-Co distance, and effectively reduces the electronic interaction with the Gr layer. The graphene Dirac cone, disrupted by the hybridization with the Co states around the Fermi energy, is restored upon O intercalation. The graphene bands recover their free-standing character except for a small *p* doping of graphene since its Dirac cone is now located slightly above the Fermi energy, in excellent agreement with ARPES [28]

and PEEM [29] measurements reported for Gr/Co(0001). In the case of Gr/Co 1ML/Ir(111), which presents a moiré pattern, the presence of the O atoms changes locally the Gr-Co distance.

We have shown that, playing with the O distribution and the continuous change of the graphene-Co registry, it is possible to tune both graphene corrugation and its electronic properties. These results support the idea that O intercalation on Gr/Co interfaces, shown experimentally to be a reversible process [29], could be used to tune the Gr-Co structural and electronic properties, which depend on both on the O concentration and surface distribution.

ACKNOWLEDGMENTS

We acknowledge stimulating discussions with M.G. Betti, C. Mariani and G. Avvisati. This work was partially supported by the MaX – Materials design at the eXascale – European Centre of Excellence, funded by the European Union program H2020-INFRAEDI-2018-1 (Grant No. 824143). Computational time on the Marconi100 machine at CINECA was provided by the Italian ISCRa program.

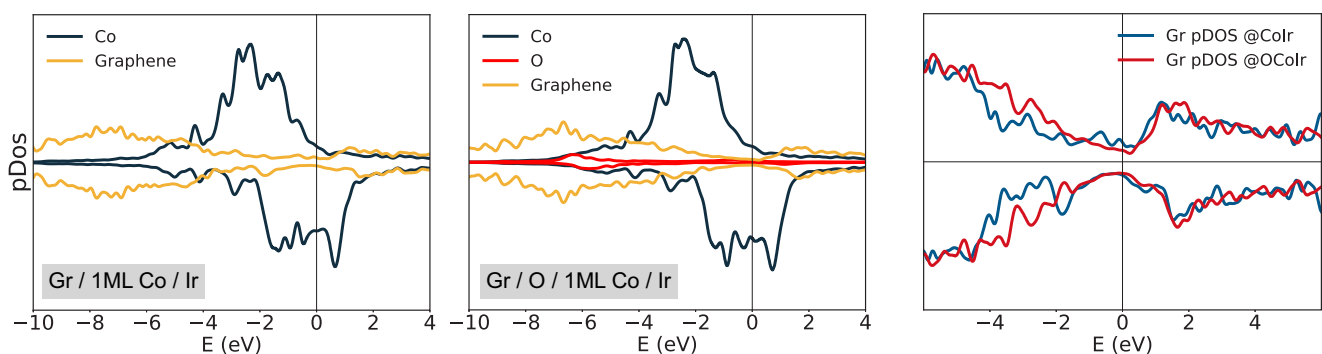


FIG. 7. Density of states computed for Gr/1ML Co/Ir, without O (first plot) and with an O concentration of 11% (second plot) and projected on the Co, C, and O atomic orbitals. The third plot compares the Gr pDOS of the two systems.

- [1] L. V. Dzemyantsova, M. Karolak, F. Lofink, A. Kubetzka, B. Sachs, K. von Bergmann, S. Hankemeier, T. O. Wehling, R. Frömter, H. P. Oepen, A. I. Lichtenstein, and R. Wiesendanger, Multiscale magnetic study of Ni(111) and graphene on Ni(111), *Phys. Rev. B* **84**, 205431 (2011).
- [2] R. Decker, J. Brede, N. Atodiresei, V. Caciuc, S. Blügel, and R. Wiesendanger, Atomic-scale magnetism of cobalt-intercalated graphene, *Phys. Rev. B* **87**, 041403(R) (2013).
- [3] D. Pacilè, P. Leicht, M. Papagno, P. Sheverdyayeva, P. Moras, C. Carbone, K. Krausert, L. Zielke, M. Fonin, Y. Dedkov, F. Mittendorfer, J. Doppler, A. Garhofer, and J. Redinger, Artificially Lattice-Mismatched Graphene/Metal Interface: Graphene/Ni/Ir(111), *Phys. Rev. B* **87**, 035420 (2013).
- [4] A. Varykhalov, D. Marchenko, J. Sánchez-Barriga, M. R. Scholz, B. Verberck, B. Trauzettel, T. O. Wehling, C. Carbone, and O. Rader, Intact dirac cones at broken sublattice symmetry: Photoemission study of graphene on Ni and Co, *Phys. Rev. X* **2**, 041017 (2012).
- [5] D. Pacilè, S. Lisi, I. Di Bernardo, M. Papagno, L. Ferrari, M. Pisarra, M. Caputo, S. K. Mahatha, P. M. Sheverdyayeva, P. Moras, P. Lacovig, S. Lizzit, A. Baraldi, M. G. Betti, and C. Carbone, Electronic structure of graphene/Co interfaces, *Phys. Rev. B* **90**, 195446 (2014).
- [6] G. Avvisati, S. Lisi, P. Gargiani, A. Della Pia, O. De Luca, D. Pacilè, C. Cardoso, D. Varsano, D. Prezzi, A. Ferretti, and M. G. Betti, FePc adsorption on the moiré superstructure of graphene intercalated with a Co layer, *J. Phys. Chem. C* **121**, 1639 (2017).
- [7] G. Avvisati, C. Cardoso, D. Varsano, A. Ferretti, P. Gargiani, and M. G. Betti, Ferromagnetic and antiferromagnetic coupling of spin molecular interfaces with high thermal stability, *Nano Lett.* **18**, 2268 (2018).
- [8] L. Massimi, S. Lisi, D. Pacilè, C. Mariani, and M. G. Betti, Interaction of iron phthalocyanine with the graphene/Ni (111) system, *Beilstein J. Nanotechnol.* **5**, 308 (2014).
- [9] D. Usachov, A. Fedorov, M. M. Otrokov, A. Chikina, O. Vilkov, A. Petukhov, A. G. Rybkin, Y. M. Koroteev, E. V. Chulkov, V. K. Adamchuk, A. Grüneis, C. Laubschat, and D. V. Vyalikh, Observation of single-spin dirac fermions at the graphene/ferromagnet interface, *Nano Lett.* **15**, 2396 (2015).
- [10] H. Vita, St. Böttcher, P. Leicht, K. Horn, A. B. Shick, and F. Máca, Electronic structure and magnetic properties of cobalt intercalated in graphene on Ir(111), *Phys. Rev. B* **90**, 165432 (2014).
- [11] J. Coraux, A. T. N'Diaye, N. Rougemaille, C. Vo-Van, A. Kimouche, H.-X. Yang, M. Chshiev, N. Bendiab, O. Fruchart, and A. K. Schmid, Air-protected epitaxial graphene/ferromagnet hybrids prepared by chemical vapor deposition and intercalation, *J. Phys. Chem. Lett.* **3**, 2059 (2012).
- [12] M. Cattelan, G. W. Peng, E. Cavaliere, L. Artiglia, A. Barinon, L. T. Røling, M. Favaro, I. Píř, S. Nappini, E. Magnano, F. Bondino, L. Gavioli, S. Agnoli, M. Mavrikakis, and G. Granozzi, The nature of the Fe-graphene interface at the nanometer level, *Nanoscale* **7**, 2450 (2015).
- [13] A. Lodesani, A. Picone, A. Brambilla, D. Giannotti, M. S. Jagadeesh, A. Calloni, G. Bussetti, G. Berti, M. Zani, M. Finazzi, L. Duò, and F. Ciccacci, Graphene as an ideal buffer layer for the growth of high-quality ultrathin Cr₂O₃ layers on Ni (111), *ACS Nano* **13**, 4361 (2019).
- [14] C. Cardoso, G. Avvisati, P. Gargiani, M. Sbroscia, M. S. Jagadeesh, C. Mariani, D. A. Leon, D. Varsano, A. Ferretti, and M. G. Betti, Magnetic response and electronic states of well defined graphene/Fe/Ir(111) heterostructure, *Phys. Rev. Materials* **5**, 014405 (2021).
- [15] M. M. Otrokov, I. I. Klimovskikh, F. Calleja, A. M. Shikin, O. Vilkov, A. G. Rybkin, D. Estyunin, S. Muff, J. H. Dil, A. L. Vázquez de Parga, R. Miranda, H. Ochoa, F. Guinea, J. I. Cerdá, E. V. Chulkov, and A. Arnau, Evidence of large spin-orbit coupling effects in quasi-free-standing graphene on Pb/Ir(111), *2D Mater.* **5**, 035029 (2018).
- [16] J. Brede, J. Sławińska, M. Abadia, C. Rogero, J. E. Ortega, I. Piquero-Zulaica, J. Lobo-Checa, A. Arnau, and J. I. Cerdá, Tuning the graphene on Ir(111) adsorption regime by Fe/Ir surface-alloying, *2D Mater.* **4**, 015016 (2016).
- [17] G. Avvisati, P. Gargiani, C. Mariani, and M. G. Betti, Tuning the Magnetic Coupling of a Molecular Spin Interface via Electron Doping, *Nano Lett.* **21**, 666 (2021).
- [18] Y. Wang, Z. Wang, J. Yang, and Xiaoguang Li, Precise Spin Manipulation of Single Molecule Positioning on Graphene by Coordination Chemistry, *J. Phys. Chem. Lett.* **11**, 9819 (2020).
- [19] E. Sierda, M. Elsebach, R. Wiesendanger, and M. Bazarnik, Probing Weakly Hybridized Magnetic Molecules by Single-Atom Magnetometry, *Nano Lett.* **19**, 9013 (2019).
- [20] G. Avvisati, P. Gargiani, P. Mondelli, F. Presel, L. Bignardi, A. Baraldi, and M. G. Betti, Metal phthalocyanines interaction with Co mediated by a moiré graphene superlattice, *J. Chem. Phys.* **150**, 054704 (2019).
- [21] F. Vincent and M. Figlarz, Quelques précisions sur les paramètres cristallins et l'intensité des raies debye-scherrer du cobalt cubique et du cobalt hexagonal, *C. R. Hebd Séances Acad Sci. C* **264**, 1270 (1967).
- [22] W. Jauch, M. Reehuis, H. J. Bleif, F. Kubanek, and P. Pattison, Crystallographic symmetry and magnetic structure of CoO, *Phys. Rev. B* **64**, 052102 (2001).
- [23] M. Pozzo, D. Alfè, P. Lacovig, P. Hofmann, S. Lizzit, and A. Baraldi, Thermal Expansion of Supported and Freestanding Graphene: Lattice Constant Versus Interatomic Distance, *Phys. Rev. Lett.* **106**, 135501 (2011).
- [24] C. Busse, P. Lazić, R. Djemour, J. Coraux, T. Gerber, N. Atodiresei, V. Caciuc, R. Brako, A. T. N'Diaye, S. Blügel, J. Zegenhagen, and T. Michely, Graphene on Ir(111): Physisorption with Chemical Modulation, *Phys. Rev. Lett.* **107**, 036101 (2011).
- [25] J. W. Arblaster, Crystallographic properties of iridium, *Platinum Metals Rev.* **54**, 93 (2010).
- [26] E. Voloshina, N. Berdunov, and Y. Dedkov, Restoring a nearly free-standing character of graphene on Ru(0001) by oxygen intercalation, *Sci. Rep.* **6**, 20285 (2016).
- [27] L. Bignardi, P. Lacovig, M. M. Dalmiglio, F. Orlando, A. Ghafari, L. Petaccia, A. Baraldi, R. Larciprete, and S. Lizzit, Key role of rotated domains in oxygen intercalation at graphene on Ni (111), *2D Mater.* **4**, 025106 (2017).
- [28] Dmitry Yu Usachov, Valery Yu Davydov, V. S. Levitskii, V. O. Shevelev, D. Marchenko, B. V. Senkovskiy, Oleg Yu Vilkov, A. G. Rybkin, L. V. Yashina, E. V. Chulkov, Irina Yu Sklyadneva, Rolf Heid, Klaus Peter Bohnen, Clemens Laubschat, and D. V. Vyalikh, Raman spectroscopy of lattice-matched graphene on strongly interacting metal surfaces, *ACS Nano* **11**, 6336 (2017).
- [29] M. Jugovac, F. Genuzio, T. O. Menteş, A. Locatelli, G. Zamborlini, V. Feyer, and C. M. Schneider, Tunable coupling

- by means of oxygen intercalation and removal at the strongly interacting graphene/cobalt interface, *Carbon* **163**, 341 (2020).
- [30] H.-Y. Ho, J.-S. Tsay, and Y.-S. Chen, Oxygen adsorption and magnetic properties of ultrathin Co/Ir(111) films, *Jp. J. App. Phys.* **49**, 075802 (2010).
- [31] S. H. Ma, Z. Y. Jiao, T. X. Wang, and X. Q. Dai, First-principles studies of oxygen chemisorption on Co(0001), *Surf. Sci.* **619**, 90 (2014).
- [32] S. Förster, G. Baum, M. Müller, and H. Steidl, Oxygen adsorption on Fe/W(110) and Co/W(110) thin films: Surface magnetic properties, *Phys. Rev. B* **66**, 134427 (2002).
- [33] M. Getzlaff, D. Egert, P. Rappolt, M. Wilhelm, H. Steidl, G. Baum, and W. Raith, Surface magnetic properties of oxygen on ferromagnetic films: a spin resolved MDS study, *Surf. Sci.* **331–333**, 1404 (1995).
- [34] J. S. Tsay and Y. S. Chen, Oxygen adsorption on ultrathin Co/Ir(111) films: Compositional anomaly, *Surf. Sci.* **600**, 3555 (2006).
- [35] P. Giannozzi, S. Baroni, N. Bonini, M. Calandra, R. Car, C. Cavazzoni, D. Ceresoli, G. L. Chiarotti, M. Cococcioni, I. Dabo, A. Dal Corso, S. de Gironcoli, S. Fabris, G. Fratesi, R. Gebauer, U. Gerstmann, C. Gougoussis, A. Kokalj, M. Lazzeri, L. Martin-Samos, N. Marzari *et al.* QUANTUM ESPRESSO: A modular and open-source software project for quantum simulations of materials, *J. Phys.: Condens. Matter* **21**, 395502 (2009).
- [36] P. Giannozzi, O. Andreussi, T. Brumme, O. Bunau, M. Buongiorno Nardelli, M. Calandra, R. Car, C. Cavazzoni, D. Ceresoli, M. Cococcioni, N. Colonna, I. Carnimeo, A. Dal Corso, S. de Gironcoli, P. Delugas, R. A. DiStasio, A. Ferretti, A. Floris, G. Fratesi, G. Fugallo, R. Gebauer, U. Gerstmann, *et al.*, E. Küçükbenli, A. Otero de-la Roza, and Advanced capabilities for materials modelling with Quantum ESPRESSO, *J. Phys.: Condens. Matter* **29**, 465901 (2017).
- [37] J. P. Perdew, K. Burke, and M. Ernzerhof, Generalized Gradient Approximation Made Simple, *Phys. Rev. Lett.* **77**, 3865 (1996).
- [38] S. Grimme, J. Antony, S. Ehrlich, and H. Krieg, A consistent and accurate *ab initio* parametrization of density functional dispersion correction (DFT-D) for the 94 elements H-Pu, *J. Chem. Phys.* **132**, 154104 (2010).
- [39] See Supplemental Material at <http://link.aps.org/supplemental/10.1103/PhysRevMaterials.6.064004> for a detailed description of the computational method, in particular for the comparison between ultra-soft and norm conserving pseudo-potentials, convergence parameters such as vacuum space between replicas, and number of layers in the model slab. See also the description of the method to obtain the correct magnetic ground state, adsorption energies of sub surface adsorption configurations, antiferromagnetic O configurations, the effect of the slab passivation with H, and the effect of possible dipoles and dipole corrections due to the difference between the two slab surfaces.
- [40] D. Pacilé, C. Cardoso, G. Avvisati, I. Vobornik, C. Mariani, D. A. Leon, P. Bonfà, D. Varsano, A. Ferretti, and M. G. Betti, Narrowing of d bands of fcco layers intercalated under graphene, *Appl. Phys. Lett.* **118**, 121602 (2021).
- [41] M. Cococcioni and S. de Gironcoli, Linear response approach to the calculation of the effective interaction parameters in the LDA + U method, *Phys. Rev. B* **71**, 035105 (2005).
- [42] W. Zhang, K. Koepf, M. Richter, and H. Eschrig, Magnetic phase transition in CoO under high pressure: A challenge for LSDA+U, *Phys. Rev. B* **79**, 155123 (2009).
- [43] P. A. Ignatiev, N. N. Negulyaev, D. I. Bazhanov, and V. S. Stepanyuk, Doping of cobalt oxide with transition metal impurities: *Ab initio* study, *Phys. Rev. B* **81**, 235123 (2010).
- [44] V. I. Anisimov, J. Zaanen, and O. K. Andersen, Band theory and mott insulators: Hubbard U instead of stoner I, *Phys. Rev. B* **44**, 943 (1991).
- [45] F. Tran, P. Blaha, K. Schwarz, and P. Novák, Hybrid exchange-correlation energy functionals for strongly correlated electrons: Applications to transition-metal monoxides, *Phys. Rev. B* **74**, 155108 (2006).
- [46] U. D. Wdowik and K. Parlinski, Lattice dynamics of CoO from first principles, *Phys. Rev. B* **75**, 104306 (2007).
- [47] A. Calloni, G. Bussetti, G. Avvisati, M. S. Jagadeesh, D. Pacilé, A. Ferretti, D. Varsano, C. Cardoso, L. Duò, F. Ciccacci, and M. G. Betti, Empty electron states in cobalt-intercalated graphene, *J. Chem. Phys.* **153**, 214703 (2020).
- [48] P. Bonfà, <https://bitbucket.org/bonfus/unfold-x>.
- [49] M. Scardamaglia, S. Lisi, S. Lizzit, A. Baraldi, R. Larciprete, C. Mariani, and M. G. Betti, Graphene-induced substrate decoupling and ideal doping of a self-assembled iron-phthalocyanine single layer, *J. Phys. Chem. C* **117**, 3019 (2013).
- [50] D. A. Duncan, N. Atodiresei, S. Lisi, P. J. Blowey, V. Caciuc, J. Lawrence, T.-L. Lee, M. G. Betti, P. K. Thakur, A. Della Pia, S. Blügel, G. Costantini, and D. Phil Woodruff, Corrugated graphene exposes the limits of a widely used *ab initio* van der Waals DFT functional, *Phys. Rev. Materials* **3**, 124001 (2019).